

Properties of ^4He in one dimension

E. Krotscheck

Institut für Theoretische Physik, Johannes Kepler Universität, A 4040 Linz, Austria

M. D. Miller

*Institut für Theoretische Physik, Johannes Kepler Universität, A 4040 Linz, Austria
and Department of Physics, Washington State University, Pullman, Washington 99164-2814*

(Received 30 March 1999; revised manuscript received 11 June 1999)

It has been suggested recently that ^4He can be prepared and studied as a quasi-one-dimensional quantum fluid. In this paper we calculate the static and dynamic properties of one-dimensional ^4He using variational methods based upon the Jastrow-Feenberg wave function and its extension to dynamic systems with time-dependent, correlated wave functions. We calculate the zero temperature equation of state and show that in one dimension ^4He is just barely self-bound with a binding energy of 0.002 K at a density of 0.036 \AA^{-1} . We calculate the Feynman excitation spectrum and corrections that contain multiphonon processes and study the density dependence of the roton feature as well as the static response function. In addition we demonstrate the presence of strong anomalous dispersion in the phonon regime. Finally, we introduce a ^3He impurity and calculate the zero concentration chemical potential as a function of ^4He linear density. We also compute the ^3He - ^3He effective interaction in the ^4He background and compute the energy of dimerization.

[S0163-1829(99)01241-2]

I. INTRODUCTION

Because of its macroscopic quantum behavior ^4He has been one of the most intensely studied many-body systems. The physics responsible for this remarkable behavior, the balance of kinetic energy to potential energy and the importance of strong *short-ranged* correlations, also make the system very difficult to treat theoretically. During the period of the 1980's, two approaches showed they were able to yield quantitative understanding of the ground-state properties of bulk (three-dimensional, homogeneous) ^4He . One approach coupled the development of powerful numerical techniques to the development of powerful computers. The other approach is the variational method based on Feenberg's correlated basis functions (CBF) theory.¹ During the last decade as interest in two-dimensional and inhomogeneous quantum liquids soared, these two basic approaches once more formed the underpinnings of our theoretical understanding. Very recently there has been some experimental^{2,3} and theoretical^{4,5} interest in the properties of ^4He in *one* dimension. In this paper we shall apply the Jastrow-Feenberg variational method to calculate the static and dynamic properties of quasi-one-dimensional ^4He . For reviews of the application of these techniques to ^4He in higher dimensions we refer the reader to Refs. 1, 6, and 7.

In recent work,⁸ the variational approach to be used in this work was applied to three model, one-dimensional, many-boson systems: hard rods, the Morse potential and the Lennard-Jones potential. We showed that the variational energies agree to better than 4% with the energies of the exactly known hard rod system. We examined the Morse system with its exactly solvable two-body Hamiltonian for the effects of dimerization on the many-body ground-state. This analysis indicated that, for these types of systems, the existence of a many-body bound state (a zero pressure, finite

density system with negative energy) only occurs if there is also a dimer. The Lennard-Jones 6-12 potential is an old model for ^4He . We showed that in the Lennard-Jones approximation one-dimensional ^4He has *no* many-body bound state and, also, it has no dimer. In this work, we utilize the modern Aziz potential⁹ and show that a dimer and a many-body bound state both exist. All three model systems showed signs of a high density transition from a liquid to a solid. In higher dimensions the onset of this phase transition was signaled by an inability to obtain convergent solutions from the variational equations for a homogeneous ground-state beyond some maximum density. We find this same instability with the Aziz potential and we tentatively identify the region as the onset of a one-dimensional standing density wave. In one dimension such a phase transition can occur only at absolute zero temperature.

The ^4He filled channels studied recently by the authors of Ref. 2 were composed of a material they denoted as FSM-16. The substance was reported to consist of a honeycomb of hexagonally shaped tubes approximately 18 Å in diameter with an undisclosed length. Thus, the geometry of the real system is characterized by tubes with one macroscopic spatial dimension and two transverse microscopic spatial dimensions. This type of system is termed *quasi* one dimensional. In an exact theory of such tubes, the motions which are transverse and parallel to the macroscopic dimension do not separate simply and are correlated. Such geometries can be treated microscopically within the extension of the Jastrow-Feenberg variational method to inhomogeneous geometries,^{10,11} but the uncertainties due to the large variety of possible geometries and interactions with the channel walls rather suggests a focused effort with a careful exploration of the possibilities within reasonable physical limits.

In Sec. II we introduce a one-dimensional ^4He Hamiltonian with the Aziz potential⁹ used for the helium-helium

interparticle interaction. The potential parameters are determined by bulk helium measurements. The Aziz potential has been used successfully to calculate static and dynamic properties of inhomogeneous and two-dimensional ^4He . In this section, we briefly describe the hypernetted-chain Euler-Lagrange (HNC-EL) formalism and then discuss the equation of state.

We next (Sec. III) turn to the excitations. We describe excitations by introducing *time-dependent* correlated variational wave functions which are the natural generalization of our static ground-state theory. Over the density regime where the liquid is stable, we find a dramatic change of the nature of the excitations from a quasifree spectrum around the saturation density, to a typical phonon-roton spectrum at high densities. We also calculate the static density-density response function and demonstrate that the above mentioned phase transition corresponds indeed to the softening of a mode with finite wave vector.

In Sec. IV we introduce a ^3He impurity and calculate the impurity binding energy and the ^3He - ^4He distribution functions. We then introduce a second ^3He impurity and compute the effective interaction between the ^3He atoms due to their direct interaction and that induced by their presence in the ^4He medium. This interaction can then be used to calculate the ^3He -dimer binding energy.

Each of these sections begins with a ‘‘theory’’ subsection where a brief outline of the relevant theory is presented. These are then followed by a ‘‘results’’ subsection containing a discussion of the computations. Each section contains references to the existing literature where the interested reader can find detailed derivations. Section V is the conclusion.

II. THE GROUND STATE

A. Theory

The ^4He Hamiltonian can be written

$$H = -\frac{\hbar^2}{2m_4} \sum_{i=1}^{N_4} \frac{d^2}{dz_i^2} + \sum_{i<j} v(|z_i - z_j|). \quad (2.1)$$

The system consists of N_4 ^4He atoms which uniformly fill a tube of length L . The particles in the tube are treated as a one-dimensional many-boson system whose interaction has the residual three-dimensional Aziz form.

The ground-state wave function is written as a variational ansatz of the Jastrow-Feenberg form

$$\Psi(z_1, \dots, z_{N_4}) = \exp \left\{ \frac{1}{2} \left[\sum_{i<j} u_2(z_i, z_j) + \sum_{i<j<k} u_3(z_i, z_j, z_k) + \dots \right] \right\}. \quad (2.2)$$

The most important component of the variational wave function is the two-body function $u_2(z_i, z_j)$, which describes both the short- and long-range correlations between pairs of particles. In fact, one of the reasons for the success of the variational theory is that it is *exact* in both the weakly interacting limit (in which case the theory reduces to the random phase

approximation) *and* in the strongly interacting limit (in which case it reduces to the Bethe-Goldstone equation).

An important aspect of the variational theory is the optimization of the correlations. The n -body functions u_n are determined by the minimization of the energy-expectation value, formally written as

$$\frac{\delta}{\delta u_n} \left[\frac{\langle \Psi_0 | H | \Psi_0 \rangle}{\langle \Psi_0 | \Psi_0 \rangle} \right] = 0, \quad n=2,3. \quad (2.3)$$

The additional information needed to solve these equations is the connection between the correlated wave functions and the physically observable distribution functions. This connection is provided by the hypernetted-chain (HNC) equations.¹ These equations are derived by diagrammatic analysis of the two-body distribution function $g(z)$ in terms of the two-body correlation function. The analysis leads to the HNC relationships

$$g(z) = \exp[u_2(z) + N(z) + E(z)]. \quad (2.4)$$

The function $E(z)$ represents an infinite series of ‘‘elementary’’ diagrams which can be expressed as multidimensional integrals involving $g(z)$. The sum of nodal diagrams $N(z)$ can be expressed conveniently in momentum space. Introducing the dimensionless Fourier transform

$$\tilde{f}(k) = \rho \int dz f(z) e^{ikz}, \quad (2.5)$$

where ρ denotes the linear density, then the function $\tilde{N}(k)$ has the form

$$\tilde{N}(k) = \frac{[S(k) - 1]^2}{S(k)}, \quad (2.6)$$

where the static structure function is defined by

$$S(k) = 1 + \rho \int_{-\infty}^{\infty} dz e^{ikz} [g(z) - 1]. \quad (2.7)$$

The level of the HNC approximation is defined by the choice of $E(z)$; e.g., HNC/0 neglects the elementary diagrams altogether, note that triplet correlations can be implemented through a modification of the definition of ‘‘elementary diagrams.’’ The combination of the HNC equations (2.4) and the Euler equations (2.3) are generally referred to as the hypernetted-chain Euler-Lagrange (HNC-EL) theory. With the quantities introduced above, the correlation energy can be written as

$$E = E_r + E_k + E_e + E_3 \quad (2.8)$$

with

$$\frac{E_r}{N} = \frac{\rho}{2} \int_{-\infty}^{\infty} dz \left[[g(z) - 1] v(z) + \frac{\hbar^2}{m} \left| \frac{d}{dz} \sqrt{g(z)} \right|^2 \right], \quad (2.9)$$

$$\frac{E_k}{N} = -\frac{1}{4} \int_{-\infty}^{\infty} \frac{dk}{(2\pi\rho)} t(k) [S(k) - 1] \tilde{N}(k), \quad (2.10)$$

$$\frac{E_e}{N} = -\frac{1}{4} \int_{-\infty}^{\infty} \frac{dk}{(2\pi\rho)} t(k) [S(k) - 1] \tilde{E}(k), \quad (2.11)$$

where $t(k) = \hbar^2 k^2 / 2m$ is the kinetic energy of a free particle, E_3 is the contribution from triplet correlations. This term can be expressed in terms of the three-body correlation function $u_3(z_1, z_2, z_3)$ and the three-body distribution function. In Refs. 12–14, working formulas and a scaling procedure for elementary diagrams have been established that have been successful in a wide range of applications.

The details of the HNC-EL scheme have been discussed in many contexts, for a comprehensive review of the method see Ref. 15. The Euler-Lagrange equation can be conveniently written in coordinate space for the radial distribution function

$$-\frac{\hbar^2}{m} \frac{d^2}{dz^2} \sqrt{g(z)} + [v(z) + \Delta V_{\text{ele}}(z) + w_1(z)] \sqrt{g(z)} = 0, \quad (2.12)$$

where the ‘‘induced interaction’’ is

$$\begin{aligned} \tilde{w}_1(k) &= -t(k)[S(k) - 1] - \frac{1}{2}t(k) \left[\frac{1}{S^2(k)} - 1 \right] \\ &= -t(k)[S(k) - 1] - \tilde{V}_{p-h}(k), \end{aligned} \quad (2.13)$$

and $\Delta V_{\text{ele}}(z)$ is a term that arises from triplet correlations and elementary diagrams,

$$\Delta V_{\text{ele}}(z) = \frac{2}{N\rho} \frac{\delta(E_3 + E_e)}{\delta g(z)}. \quad (2.14)$$

The coordinate-space formulation of the Euler equation (2.12) is readily identified with the boson Bethe-Goldstone equation, which sums the dominant diagrams in the strong-coupling limit.

A momentum space formulation of the Euler equations equivalent to (2.12) can be given in terms of the structure factor $S(k)$,

$$S(k) = \left[1 + \frac{2}{t(k)} \tilde{V}_{p-h}(k) \right]^{-1/2}. \quad (2.15)$$

This equation is formally identical to the boson-RPA expression for the structure factor; the HNC-EL theory supplements the RPA with a microscopic theory of the particle-hole interaction

$$\begin{aligned} V_{p-h}(z) &= g(z)[v(z) + \Delta V_{\text{ele}}(z)] + \frac{\hbar^2}{m} \left| \frac{d}{dz} \sqrt{g(z)} \right|^2 \\ &+ [g(z) - 1]w_1(z). \end{aligned} \quad (2.16)$$

Thus the HNC-EL theory sums *both* important sets of diagrams self-consistently.

Equations (2.15), (2.16), and (2.13) can be solved iteratively for $g(z)$ and $S(k)$. We can then go back and calculate the ground-state energy from the expression (2.8) for the energy-expectation value.

The pressure of the system is calculated by varying the energy per particle with respect to the density. It can be expressed entirely in terms of the ground-state structure functions

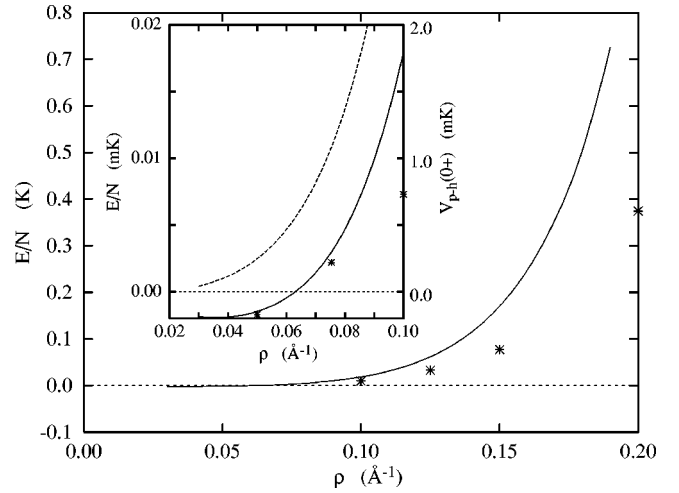


FIG. 1. The figure shows the equation of state of one-dimensional ^4He , a magnified picture of the area around saturation density is shown in the inset. Asterisks in the inset show results of Ref. 5.

$$\frac{P}{\rho} = \rho \frac{dE/N}{d\rho}. \quad (2.17)$$

The chemical potential of the system is defined as $\mu = E/N + P/\rho$, and the hydrodynamic compressibility K_T is obtained by differentiating the chemical potential with respect to density

$$m c_s^2 = \frac{1}{\rho K_T} = \rho \frac{d\mu}{d\rho}, \quad (2.18)$$

where c_s is the isothermal speed of sound. For the adsorbed systems, c_s should be interpreted as fourth sound¹⁶ since presumably the pore size will be significantly smaller than the viscous penetration depth in the hydrodynamic limit. Since the definition of the compressibility contains the second derivative of the energy one also needs to calculate the linear response of the ground-state structure functions to density variations. We will return to this problem when the static response function is evaluated.

B. Results

In Fig. 1 we show the zero-temperature equation of state of one dimensional ^4He . We find that, in one dimension, ^4He is self-bound at zero pressure. The binding energy is 0.002 K at a density of 0.036 \AA^{-1} . The existence of a many-body bound state is in agreement with our previous work which indicated that if the system dimerizes then it will also have a many-body bound state. By solving the two-body Schrödinger equation with the Aziz potential we have found a two-body bound state with total energy = -0.83 mK and an average particle-particle separation of 64 \AA . Newer potentials^{17,18} give the slightly lower binding energies of -1.68 mK and -1.78 mK , respectively. The low density and small value of the binding energy necessitated great care in the numerical work for both the two-body and many-body systems. As shown in Fig. 1, we found solutions for densities in the range $0.03 \text{ \AA}^{-1} < \rho < 0.19 \text{ \AA}^{-1}$; by very cautious iterations one might be able to decrease the lowest density, and increase the highest density, slightly.

The range of densities where solutions of the HNC-EL equations are found is determined by the onset of physical instabilities. The low density instability is a *spinodal point* separating the self-bound liquid from a zero-density gas; it is determined by the density where $\tilde{V}_{p-h}(0+)$ vanishes. The instability is seen in Eq. (2.15); in order to have a real $S(k)$, we must have $\tilde{V}_{p-h}(0+) > 0$.

The inset of Fig. 1 shows a magnified picture of the density region around saturation. Going below saturation density, one quickly approaches the spinodal point. In principle, the long-wavelength limit of $\tilde{V}_{p-h}(k)$ is equal to the hydrodynamic compressibility (2.18). In practice, however, the macroscopic quantity (2.18) and the microscopic quantity $\tilde{V}_{p-h}(0+)$ are identical only in an exact theory. The calculation of the hydrodynamic compressibility through macroscopic derivatives (2.17) and (2.18), is normally more accurate than using the small- k limit of Eq. (2.15). Both in two and in three dimensions it was found¹⁹ that the inconsistency between Eq. (2.18) and $\tilde{V}_{p-h}(0+)$ is not very severe in the vicinity of the spinodal point. The inset in Fig. 1 also shows $\tilde{V}_{p-h}(0+)$ at low densities, by extrapolating $\tilde{V}_{p-h}(0+)$ to lower densities, we estimate that the spinodal point of the one-dimensional liquid is at $\rho_s \approx 0.022 \text{ \AA}^{-1}$. A fully consistent calculation along the lines of Ref. 19 would lower this value to perhaps 0.02 \AA^{-1} . Applying the analysis of Ref. 19 to a one-dimensional system, we find that

$$mc_s^2 \propto (\rho - \rho_s)^{2/3} \text{ as } \rho \rightarrow \rho_s. \quad (2.19)$$

As a word of caution we mention that the nonanalytic form (2.19) is valid only in a very small density regime around the spinodal point and normally does not provide a useful tool for finding the spinodal density by extrapolation.

We note that the system is, in the whole accessible regime, at relatively low density in terms of the *interparticle distance*. In three dimensions at zero pressure, the average spacing per particle is approximately 3.6 \AA whereas our saturation density corresponds to an average particle spacing of 33 \AA , and the *highest* density corresponds to a spacing of 5.3 \AA . But even at these relatively low densities, the inclusion of the contributions from the elementary diagrams and also the three-body terms made non-negligible changes in the results, in other words the system is in a sense more strongly correlated than the two- and three-dimensional analogs. In the long wavelength limit we have

$$S(k) \approx \frac{\hbar k}{2mc_s}. \quad (2.20)$$

It follows that $g(z) = 1 + \hbar/mc_s \rho z^2$ for $z \rightarrow \infty$. Hence, the kinetic energy term $|d\sqrt{g(z)}/dz|^2$ in $V_{p-h}(r)$ has the same range as the bare potential which dominates, at long distances, in both two and three dimensions.

Triplet correlations and elementary diagrams are, of course, more important at high densities. For example, at the two-body, HNC/0 level there were stable solutions found up to a density of approximately 0.22 \AA^{-1} while the inclusion of triples and elementary diagrams reduced the maximum density, for which solutions could be found, to 0.19 \AA^{-1} .

In 2D and 3D, the disappearance of solutions at high-densities can be identified as the signature of the presence of

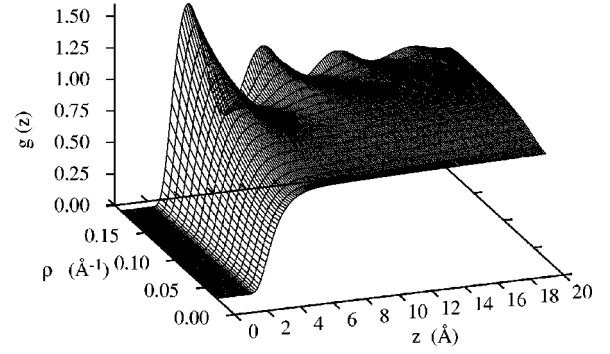


FIG. 2. The figure shows the ^4He - ^4He pair distribution function $g(z)$ as a function of interparticle distance z and density ρ . Note the development of a very typical low-density form at $\rho \approx 0.03 \text{ \AA}^{-1}$ up to the highly structured form at the highest attainable density.

a liquid-solid phase transition.^{20,21} In 1D this same conclusion is not evident and more work will be required before a definitive statement can be made that we are, or perhaps are not, seeing a transition to a state with a nonuniform density. We will return to this point in the next section where we discuss excitations and the static response function.

In Fig. 2, we show the set of ‘‘radial’’ distribution functions, $g(z)$, for one-dimensional ^4He . We note that there is considerable structure in the highest density distribution function despite the fact that relative to bulk interparticle spacings, this system is very dilute. A similar statement can be made about the static structure function $S(k)$, shown in Fig. 3. At high densities, one has a very strong peak at $k = 1.44 \text{ \AA}^{-1}$ corresponding to a pronounced structure at a length scale of 4.25 \AA which is the location of the nearest neighbor peak in $g(z)$. However, a pronounced quasi-periodic structure appears in both $g(z)$ and $S(k)$ only at densities well beyond saturation.

In Ref. 5 a diffusion Monte Carlo calculation of the equation of state for ^4He in one-dimension is reported. This calculation is consistent with our conclusion that a low-density bound state exists. Some of the Monte Carlo results in density regime $\rho \leq 0.1$ shown, for the sake of comparison, in Fig. 1. Whereas the agreement between our variational results and the simulation data is, for the two lower densities, of the expected accuracy, there is a notable discrepancy at $\rho = 0.1 \text{ \AA}^{-1}$. This apparent discrepancy is due to large cancellations between kinetic and potential energy, as seen in Table I. The table shows a breakdown of the total energy between

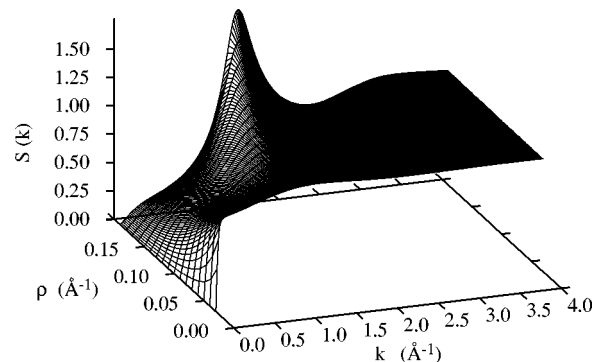


FIG. 3. Same as Fig. 2 for the *static structure function* $S(k)$. At small densities the large slope is indicative of a small value for the speed of sound.

TABLE I. A comparison between the DMC results of Ref. 5 for potential and kinetic energy (Ref. 44) with HNC-EL results. All energies are given in K, Δ is the Monte Carlo statistical uncertainty.

ρ (\AA^{-1})	$\langle V \rangle$			$\langle T \rangle$		
	DMC	Δ	HNC-EL	DMC	Δ	HNC-EL
0.100	-0.538	0.005	-0.513	0.550	0.005	0.530
0.125	-0.777	0.023	-0.756	0.813	0.023	0.812
0.150	-1.121	0.028	-1.100	1.199	0.028	1.249
0.175	-1.595	0.059	-1.581	1.791	0.062	1.932

kinetic and potential energy for both the DMC data and the HNC-EL results. The *potential* energy agrees, throughout, with our result within better than a percent, whereas the discrepancy of the kinetic energies is between one and 8%. Thus, the disagreement between our results and the simulation data of Ref. 5 is to a large extent due to the accidental cancellation of large numbers; it is consistent with the expected accuracy derived from the comparison of our results with exact results for hard rods.⁸ It is indicative of the fact that the Jastrow-Feenberg wave function (2.2) is not exact. The good agreement of the potential energies is an indication that our pair distribution functions, which are important input for our further calculations, are very good.

III. DYNAMICS

A. Theory

A plausible way to deal with excitations within the variational approach is to allow for a time dependence of the n -body functions $u_n(\mathbf{r}_1, \dots, \mathbf{r}_n)$. Beyond the time dependence of the components of the wave function, Eq. (2.2), we must also include a time-dependent one-body function since the dynamics will normally break the translational invariance. The wave function of the excited system is again written in the Jastrow-Feenberg form

$$|\Psi(t)\rangle = \frac{e^{-iE_0t/\hbar} e^{(1/2)\delta U(\mathbf{r}_1, \dots, \mathbf{r}_N;t)} |\Psi_0\rangle}{[\langle \Psi_0 | e^{\delta U} | \Psi_0 \rangle]^{1/2}}, \quad (3.1)$$

where $|\Psi_0\rangle$ is the (variational) ground state, and

$$\delta U(\mathbf{r}_1, \dots, \mathbf{r}_N;t) = \sum_i \delta u_1(\mathbf{r}_i;t) + \sum_{i<j} \delta u_2(\mathbf{r}_i, \mathbf{r}_j;t) \quad (3.2)$$

is a time-dependent complex function representing fluctuations of the n -body parts of the wave function. Since the excitations can be considered as small perturbations of the ground state, one can treat δU to the leading nontrivial order.

The time-dependent correlations are determined by the action principle^{22,23}

$$\delta J = \delta \int_{t_1}^{t_2} \mathcal{L}[\Psi(t), \dot{\Psi}(t)] dt = 0 \quad (3.3)$$

with the Lagrangian

$$\mathcal{L} = \left\langle \Psi(t) \left| H - i\hbar \frac{\partial}{\partial t} \right| \Psi(t) \right\rangle = \left\langle \Psi_0 \left| H - E_0 - i\hbar \frac{\partial}{\partial t} \right| \Psi_0 \right\rangle. \quad (3.4)$$

Minimizing the action (3.3) leads to four Euler-Lagrange equations for the real and imaginary parts of δu_1 and δu_2 which are conveniently written in the form of two continuity equations

$$\frac{\partial j_1(z_1;t)}{\partial z_1} = \dot{\rho}_1(z_1;t),$$

$$\frac{\partial j_2(z_1, z_2;t)}{\partial z_1} + (1 \leftrightarrow 2) = \dot{\rho}_2(z_1, z_2;t) \quad (3.5)$$

with the one- and two-particle currents

$$\begin{aligned} -ij_1(z_1;t) &= \frac{\hbar}{2m} \left\{ \bar{\rho}_1(z_1) \frac{\partial \delta u_1(z_1;t)}{\partial z_1} \right. \\ &\quad \left. + \int dz_2 \bar{\rho}_2(z_1, z_2) \frac{\partial \delta u_2(z_1, z_2;t)}{\partial z_1} \right\} \\ -ij_2(z_1, z_2;t) &= \frac{\hbar}{2m} \left\{ \bar{\rho}_2(z_1, z_2) \left(\frac{\partial \delta u_1(z_1;t)}{\partial z_1} \right. \right. \\ &\quad \left. \left. + \frac{\partial \delta u_2(z_1, z_2;t)}{\partial z_1} \right) \right. \\ &\quad \left. + \int dz_3 \bar{\rho}_3(z_1, z_2, z_3) \frac{\partial \delta u_2(z_1, z_3;t)}{\partial z_1} \right\}, \end{aligned} \quad (3.6)$$

where $\bar{\rho}_1$ and $\bar{\rho}_2$ are the time-independent ground-state quantities. The derivatives of the correlation functions are related to the derivatives of the pair-distribution functions through the set of exact BGY equations.¹

Note that, for the derivation of Eqs. (3.6) it is necessary to assume that correlations up to $u_4(z_1, z_2, z_3, z_4)$ have been optimized or, equivalently, that $u_4(z_1, z_2, z_3, z_4)$ is negligible. One has normally only indirect evidence that this approximation is legitimate, for example, by comparing the energetics with simulation data. In one dimension, one also can compare with exact results for the point-rod system. This was done in Ref. 8 where we found that the agreement between the exact $S(k)$ and $g(z)$ with our HNC-EL results is quite good. We expect therefore that the neglect of $u_4(z_1, z_2, z_3, z_4)$ is legitimate; in particular we feel the exactly one-dimensional system is a substantially cruder approximation for ⁴He in a nanotube than the omission of $u_4(z_1, z_2, z_3, z_4)$.

Since the relationships between the time-dependent components of the pair-correlation and pair-distribution functions involve ground-state densities up to four-body distribution function ρ_4 , approximations are necessary. Different implementations^{24,25,21} use different approximations which

are chosen depending on the problem under consideration, and on the system that is being investigated.

At this time, the best implementation of the theory in 3D and 2D is by Saarela and collaborators^{25–27} which lead to very good agreement between the theoretically predicted and the experimentally observed roton minimum. Our calculations utilize the so-called ‘‘convolution approximation,’’²⁴ the expected accuracy of this approximation will be discussed further below where we display the analytic formula.

Restricting the time dependence to the *one-body component only* leads directly to the Feynman theory of excitations²⁸ and to the dispersion relation

$$\varepsilon(k) = \frac{\hbar^2 k^2}{2mS(k)}. \quad (3.7)$$

Equation (3.7) provides an upper bound for the lowest-lying excitation and is exact in the long-wavelength limit, but is less accurate at shorter wavelengths. The cause of this deficiency is evident from the variational point of view: when the wavelength of an excitation becomes comparable to the average particle distance, one should expect that all correlations that are important at that wavelength are also time-dependent. Consequently, it was found in previous studies of liquid ${}^4\text{He}$ (Refs. 24–27,29) that much of the energetics of the excitations in the medium-to-high momentum range can be attributed to fluctuating short-ranged correlations, and the same is expected to be true in the one-dimensional system. For the implementation of the present theory of excitations and dynamic structure the structure function $S(k)$ is the essential input. This $S(k)$ is provided by our ground-state calculations described above, but it may equally well be taken from other calculations like a Monte Carlo simulation.

A convenient and mathematically transparent level beyond the Feynman approximation at which one can deal with fluctuating pair correlations is the uniform limit approximation¹ for the kernels of the equations of motion (3.5) and (3.6). In a somewhat different derivation of the dynamics, this approximation has also been used by Campbell *et al.*^{6,24} to calculate the phonon-roton spectrum in bulk liquid ${}^4\text{He}$. Important formal properties of the dynamic structure function have been discussed by Jackson.^{30–32} The equations-of-motion method has first been used in Ref. 25, the connection to the derivations of Campbell²⁴ and Jackson^{30–32} has, in the somewhat more general case of an inhomogeneous system, been derived in Refs. 29 and 33. The theory leads to a dynamic response function of the plausible form

$$\chi(k, \omega) = \frac{S(k)}{\hbar\omega - \varepsilon(k) - \Sigma(k, \omega)} + \frac{S(k)}{-\hbar\omega - \varepsilon(k) - \Sigma(k, -\omega)}, \quad (3.8)$$

where $S(k)$ is the static structure function, $\varepsilon(k)$ the Feynman excitation spectrum (3.7) and $\Sigma(k, \omega)$ is the self-energy arising from phonon-splitting and recombination processes:

$$\Sigma^{\text{CBF}}(k, \omega) = \frac{1}{2} \int \frac{dpdq}{(2\pi)\rho} \delta(k+p+q) \frac{|V_3(k;p,q)|^2}{\hbar\omega - \varepsilon(p) - \varepsilon(q)}, \quad (3.9)$$

where the three-phonon coupling matrix element is given in terms of ground-state quantities as²⁴

$$V_3(k;p,q) = \frac{\hbar^2}{2m} \sqrt{\frac{S(p)S(q)}{S(k)}} [kp\tilde{X}(p) + kq\tilde{X}(q) - k^2\tilde{u}_3(k,p,q)]. \quad (3.10)$$

In the zero-frequency limit we obtain the static response function

$$\chi^{\text{CBF}}(k, 0) = -\frac{2S(k)}{\varepsilon(k) + \Sigma^{\text{CBF}}(k, 0)}. \quad (3.11)$$

If we ignore the self-energy correction $\Sigma(k, \omega)$, the response function (3.8) reduces to the familiar response function in the random phase approximation

$$\chi^{\text{RPA}}(k, \omega) = \frac{2t(k)}{\hbar^2\omega^2 - \varepsilon^2(k)} = \frac{\chi_0(k, \omega)}{1 - \tilde{V}_{p-h}(k)\chi_0(k, \omega)} \quad (3.12)$$

with the response function of the noninteracting boson system

$$\chi_0(k, \omega) = \frac{2t(k)}{\hbar^2\omega^2 - t^2(k)}. \quad (3.13)$$

The dynamic structure factor follows immediately from the imaginary part of the dynamic response function

$$S(k, \omega) = -\frac{1}{\pi} \text{Im} \chi(k, \omega). \quad (3.14)$$

It is worth stressing that the static structure factor $S(k)$ obtained from the above response function is *identical* to both, the one obtained from the ground state calculation and the one obtained in the Feynman approximation. In other words, the self-energy correction changes the relative weight of the individual excitations and resonances, but it does not change the integrated strength. Thus, the first two energy weighted sum rules are identical whether calculated in Feynman or in CBF approximation:

$$\begin{aligned} S(k) &= \int_{-\infty}^{\infty} \frac{d\hbar\omega}{2\pi} \text{Im} \chi^{\text{RPA}}(k, \omega) \\ &= \int_{-\infty}^{\infty} \frac{d\hbar\omega}{2\pi} \text{Im} \chi^{\text{CBF}}(k, \omega), \\ \frac{\hbar^2 k^2}{2m} &= \int_{-\infty}^{\infty} \frac{d\hbar\omega}{2\pi} \hbar\omega \text{Im} \chi^{\text{RPA}}(k, \omega) \\ &= \int_{-\infty}^{\infty} \frac{d\hbar\omega}{2\pi} \hbar\omega \text{Im} \chi^{\text{CBF}}(k, \omega). \end{aligned} \quad (3.15)$$

B. Results

Excitations are conveniently discussed in terms of the dynamic structure function $S(k, \omega)$, Eq. (3.14). In the Feynman approximation, $S(k, \omega)$ is exhausted by a single mode,

$$S(k, \omega) = S(k) \delta[\hbar\omega - \varepsilon(k)] \quad (3.16)$$

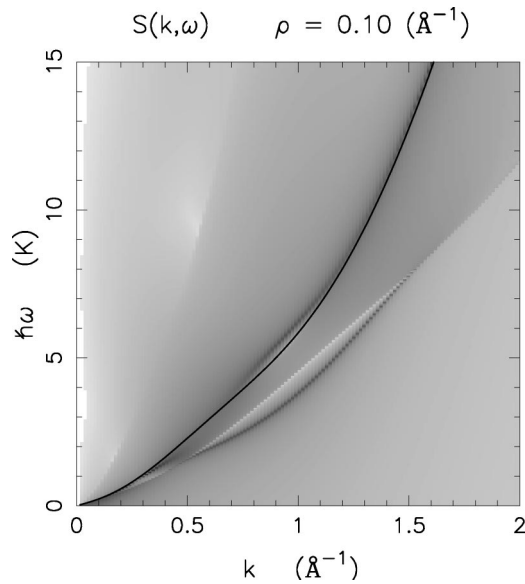


FIG. 4. Grey-scale plot of the dynamic structure function $S(k, \omega)$ at $\rho = 0.05 \text{ \AA}^{-1}$. Darker areas correspond to higher values of $S(k, \omega)$. The heavy solid line follows the Feynman approximation (3.7).

whereas it is nontrivial when the self-energy (3.9) is included. Before turning to the numerical results, we should briefly discuss the expected accuracy of the calculations. In three dimensions, the present implementation of the theory *underestimates* the consequence of including self-energy corrections by about 30%; the reason is that the energy denominator in Eq. (3.9) contains the Feynman spectrum, whereas it *should* contain a self-consistent spectrum. Artificially lowering the spectrum in the energy denominator such that it agrees roughly with the experimental phonon-roton spectrum also lowers the spectrum and produces good agreement with the experiments. In general, we consider some phenomenological input as legitimate; however, here we shall not include such modifications. We expect, therefore, that our results *underestimate* the importance of time-dependent pair correlations.

In Figs. 4–7 we show $S(k, \omega)$ for the densities 0.05, 0.10, 0.15, and 0.19 \AA^{-1} . At the lowest densities the spectrum is quadratic with little evidence of a roton minimum. This is clear from the previous results, Figs. 2 and 3. The Feynman spectrum (3.7) is, at saturation density, practically a free spectrum; a linear phonon branch persists for very long wavelengths only and is practically invisible.

A consequence of the anomalous dispersion of a quadratic excitation spectrum is that it is kinematically allowed for a single phonon to decay into two phonons. For wave vectors on the order of 1 \AA^{-1} there are no propagating collective modes because of this anomalous dispersion. Such an effect is contained in the CBF self-energy; the ridge in $S(k, \omega)$ seen at about *half* the Feynman energy in Fig. 4 reflects this effect. The strength of $S(k, \omega)$ is still distributed along the kinetic energy line, but the $S(k, \omega)$ has a finite width. Interestingly, the free spectrum remains the dominant feature up to a density of 0.15 \AA^{-1} where the first signatures of a “rotonlike” structure appear.

As the density is increased, a linear region in k appears as does a roton minimum. The minimum is quite pronounced at

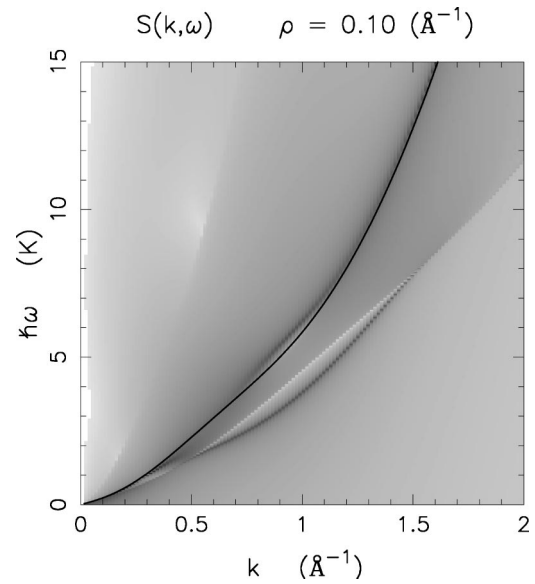


FIG. 5. Same as Fig. 4 for $\rho = 0.10 \text{ \AA}^{-1}$.

the highest density, 0.19 \AA^{-1} , with a value of 3.5 K at 1.38 \AA^{-1} . The Feynman approximation gives an upper bound for the roton minimum of 6.8 K. From experience with our calculations in 2D and 3D we suspect that our calculation still overestimates the roton energy since a renormalized energy-denominator in the self-energy (3.9) will increase the magnitude of the self-energy. Once more it is interesting that this amount of structure is appearing in a system whose average spacing is more than 5 \AA per particle.

Returning to the high-density instability of the system, we consider the static response function $\chi(k, 0)$. At the point of a phase transition, $\chi(k, 0)$ should become singular, or $1/\chi(k, 0)$ should develop a node.

Figure 8 shows the inverse static response function as a function of density and momentum transfer. At low densities, the response function is relatively featureless; it starts developing a minimum in the regime $k \approx 0.9 - 1.5 \text{ \AA}^{-1}$ corresponding roughly to the average particle distance at the relevant density. The value of $1/\chi(k_{\min}, 0)$ at its minimum

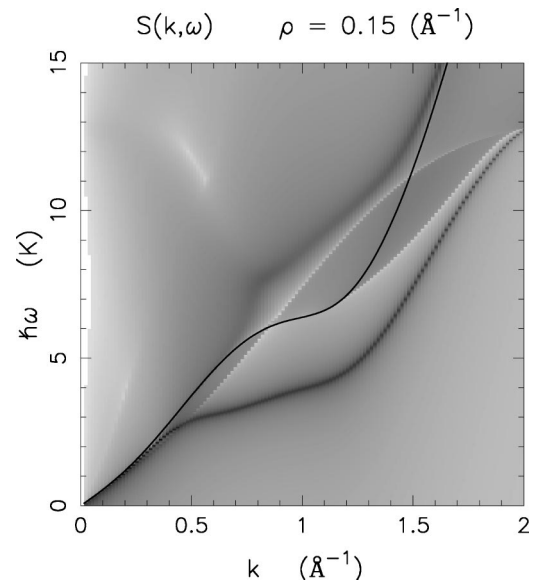


FIG. 6. Same as Fig. 4 for $\rho = 0.15 \text{ \AA}^{-1}$.

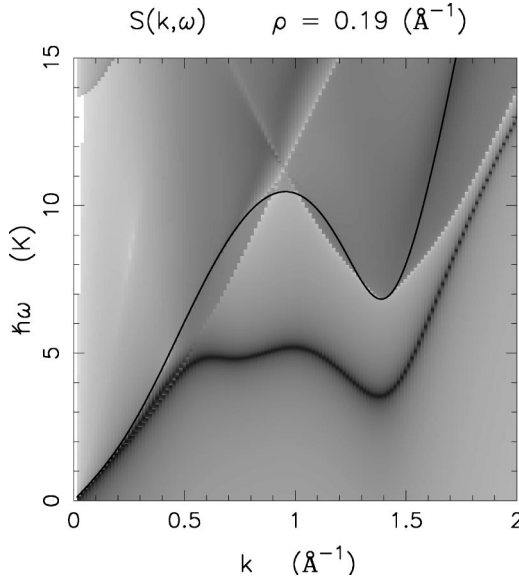


FIG. 7. Same as Fig. 4 for $\rho=0.20 \text{ \AA}^{-3}$.

and the corresponding momentum k_{\min} are shown, as a function of density, in Fig. 9. At high densities, the inverse static response function drops very rapidly; cautious extrapolation of the results of Fig. 9 suggests that it should go to zero at $\rho \approx 0.22 \text{ \AA}^{-3}$. Keeping our above remarks in mind that the present implementation of the self-energy *underestimates* its contribution, the results of Fig. 9 are consistent with our finding that solutions of the Euler equation cease to exist at $\rho \approx 0.19-0.20 \text{ \AA}^{-3}$.

IV. ^3He IMPURITIES

A. Theory

In this section we shall describe the modifications needed when one ^3He atom is added to a fluid of N_4 ^4He particles. We distinguish the ^3He from the rest of the particles by using the notation z_0 for its position in space. The Hamiltonian, H^I , contains the kinetic energy terms and the ^3He - ^4He and ^4He - ^4He interactions.

$$H^I = -\frac{\hbar^2}{2m_3} \frac{d^2}{dz_0^2} - \sum_{j=1}^{N_4} \frac{\hbar^2}{2m_4} \frac{d^2}{dz_j^2} + \sum_{j=1}^{N_4} V^{34}(|z_0 - z_j|) + \sum_{j < k}^{N_4} V^{44}(|z_j - z_k|). \quad (4.1)$$

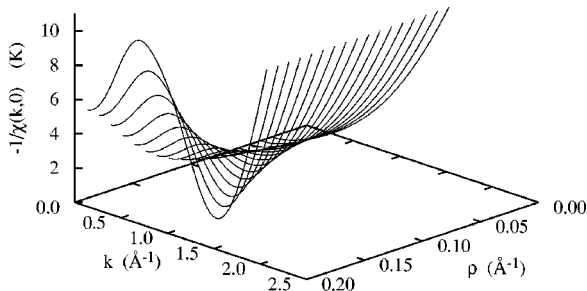


FIG. 8. The inverse static response function $-1/\chi(k,0)$ as a function of momentum and density.

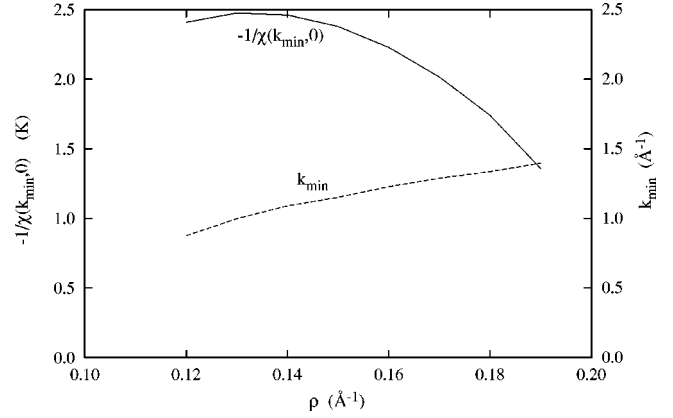


FIG. 9. The figure shows the minimum value of the inverse static response function, $-1/\chi(k_{\min},0)$ (solid line, left scale) and the location k_{\min} of that minimum (dashed line, left scale) as a function of density.

We can treat the single impurity system as the zero concentration limit of a spatially homogeneous mixture, thus we need not include a one-particle correlation function into the Jastrow-Feenberg wave function. The fact that there is only one foreign particle makes it possible to use Eq. (2.2) for the background wave function $\Psi(z_1, \dots, z_{N_4})$ and multiply that function with the correlation function between the ^3He and the ^4He background

$$\Psi^I(z_0, z_1, \dots, z_{N_4}) = \exp \left[\frac{1}{2} \left[\sum_{j=1}^{N_4} u^{34}(z_0, z_j) + \frac{1}{2!} \sum_{j \neq k}^{N_4} u^{344}(z_0, z_j, z_k) \right] \right] \times \Psi(z_1, \dots, z_{N_4}). \quad (4.2)$$

As in Sec. II, the description of the ^4He background, we include pair and triplet correlation functions.

The *chemical potential* of the ^3He is the energy gained or lost by adding one ^3He into the liquid, in other words it equals to the energy difference

$$\mu_3 = E_{N_4+1}^I - E_{N_4} = \frac{\langle \Psi^I | H^I | \Psi^I \rangle}{\langle \Psi^I | \Psi^I \rangle} - \frac{\langle \Psi | H | \Psi \rangle}{\langle \Psi | \Psi \rangle}, \quad (4.3)$$

where $E_{N_4+1}^I$ is the energy of the system of N_4 ^4He atoms and one ^3He impurity. In the calculation of the impurity chemical potential from the definition (4.3) we must include, besides the explicit terms containing impurity distribution functions, also the *changes* in the background distribution and correlation functions due to the presence of an impurity. These changes are of the order of $1/N$ and therefore cause a change of order unity in the ^4He correlation energy.

The one-particle density for the impurity is defined by integrating over all the background coordinates in the wave function

$$\rho_3(z_0) = \frac{1}{N_0} \int dz_1 \cdots dz_{N_4} |\Psi^I(z_0, \dots, z_{N_4})|^2 \equiv \frac{1}{L}; \quad (4.4)$$

it is equal to one over the *total volume* L of the system, which includes the impurity particle. Similarly, to obtain the impurity-background two-particle density, one integrates over all background coordinates except one,

$$\rho_3(z_0, z_1) = \frac{N_4}{N_0} \int dz_2 \dots dz_{N_4} |\Psi^I(z_0, z_1, \dots, z_{N_4})|^2, \quad (4.5)$$

where N_0 is the normalization integral

$$N_0 = \int dz_0 \dots dz_{N_4} |\Psi^I(z_0, \dots, z_{N_4})|^2. \quad (4.6)$$

The radial distribution function between the impurity and background particles is defined by

$$\rho_{34}(z_0, z_1) = \rho_3(z_0) \rho_4(z_1) g^{34}(z_0, z_1). \quad (4.7)$$

Note that $\rho_4(z_1)$ in Eq. (4.7) is the *pure* ^4He background density

$$\rho_4(z_1) = N_4 \frac{\int dz_2 \dots dz_{N_4} |\Psi(z_1, \dots, z_{N_4})|^2}{\int dz_1 \dots dz_{N_4} |\Psi(z_1, \dots, z_{N_4})|^2} \equiv \frac{N_4}{L_4}. \quad (4.8)$$

Definitions (4.4)–(4.8) determine the volume integral

$$\int dz_1 g^{34}(z_1, z_0) = L_4. \quad (4.9)$$

The volume occupied by one ^4He particle, $l_4 = L_4/N_4$ is different from the volume $l_3 = L - L_4$ occupied by the ^3He . This difference has consequences for the sequential relation for the ^3He - ^4He radial distribution function of Eq. (4.7)

$$\int dz_1 \rho_4(z_1) [g^{34}(z_1, z_0) - 1] = -\frac{l_3}{l_4} \equiv -\beta. \quad (4.10)$$

Here we have introduced the *volume excess factor* β , which is an important experimental parameter.³⁴

The ^3He structure function is the Fourier transform of the radial distribution function

$$S^{34}(k) = \rho_4 \int_{-\infty}^{\infty} dz e^{ikz} [g^{34}(z) - 1], \quad (4.11)$$

and its value at the origin,

$$S^{34}(0+) = -\beta, \quad (4.12)$$

is given by the sequential relation (4.10). In the definitions (4.4) and (4.8) we have taken explicit advantage of the fact that the zero concentration limit of a homogeneous mixture is formally equivalent to the one particle limit which makes it possible to take the Fourier transform with respect to the relative coordinate alone. From now on we shall ignore the coordinate argument in the density factors.

The volume excess factor is a measurable quantity and when it is well determined, as for the ^3He impurity, it can be used to calculate the ^3He chemical potential by integrating the equation

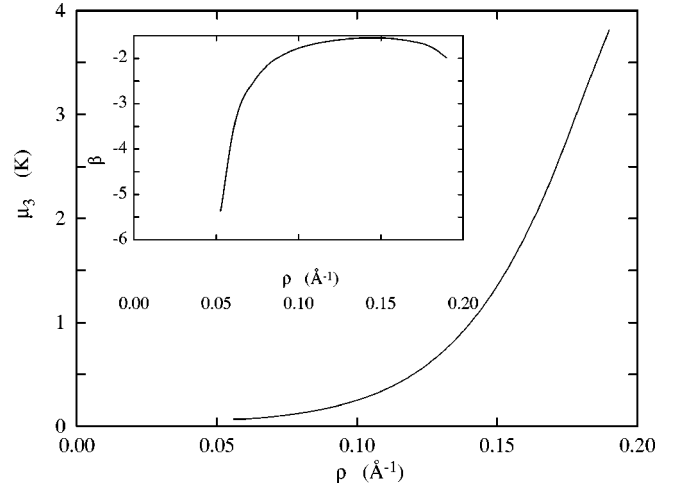


FIG. 10. The figure shows the chemical potential μ_3 of a ^3He impurity in one-dimensional ^4He as a function of the background density. The inset shows the volume factor β .

$$\beta = \rho_4(P) \frac{d\mu_3}{dP} \quad (4.13)$$

over the pressure.³⁵ These two relations can be used as a check of consistency of the theory in a similar manner as using the thermodynamic compressibility to test the consistency of the slope of the structure function in the long wavelength limit.

The remaining manipulations have been described extensively in the literature^{36,15} and shall not be repeated here.

Along the same lines, the *interaction* between pairs of ^3He impurities can also be derived.³⁷ In the dilute limit one obtains an effective Schrödinger equation for the relative wave function $\phi_{33}(z)$

$$\begin{aligned} & -\frac{\hbar^2}{m_3} \frac{d^2}{dz^2} \phi_{33}(z) + [v(z) + \Delta V_{\text{ele}}^{33}(z) + w_{33}(z)] \phi_{33}(z) \\ & = -\frac{\hbar^2}{m_3} \frac{d^2}{dz^2} \phi_{33}(z) + V_{33}(z) \phi_{33}(z) \\ & = \epsilon_{33} \phi_{33}(z), \end{aligned} \quad (4.14)$$

where the induced interaction $w_{33}(z)$ is obtained from background and single-impurity quantities,

$$\tilde{w}_{33}(k) = -\frac{\hbar^2 k^2}{2m_4} \left(\frac{S^{34}(k)}{S^{44}(k)} \right)^2 \left[2 \frac{m_4}{m_3} S^{44}(k) + 1 \right]. \quad (4.15)$$

The corrections $\Delta V_{\text{ele}}^{33}(z)$ due to elementary diagrams and triplet correlations contain topologically the same diagrams as were used in the ground-state calculation; details may again be found in Ref. 15. However, the single-impurity limit also provides useful insight into the *stability* of a mixture of ^3He and ^4He . In *three* dimension, such mixtures are stable against concentration fluctuations even in the low concentration limit. Since Eq. (4.14) is the low-concentration limit of the Euler equation of the 33 correlations in the mixture theory, it *must not* have a bound state. If the converse is true, the mixture will be unstable, first against the formation

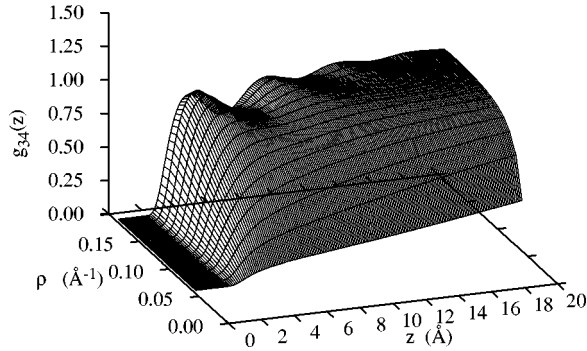


FIG. 11. The figure shows the ^4He - ^3He pair distribution function $g_{34}(z)$ as a function of interparticle distance z and density ρ . Note the very long range of the correlations at low densities; they reach out to 100 \AA at $\rho=0.05 \text{ \AA}^{-1}$.

of dimers, and then against concentration fluctuations. Indeed, such a scenario has been proposed by Bashkin and collaborators.^{38,39}

B. Results

The calculation of impurity properties was implemented at the same level as the calculation of the background quantities which is, in turn, the same as used in previous work.^{14,36,15} Results of the calculations include impurity binding energies, distribution and structure functions, and the volume factor. Figure 10 shows the energetics of the ^3He impurity. Within computational accuracy, a ^3He atom is unbound in one-dimensional liquid ^4He at all densities.

We note that in one dimension the surface state can be generated by simply removing either the right or left hand line of ^4He atoms from the vicinity of the ^3He impurity. Thus, the above result would indicate that the existence of an Andreev type of surface state is unlikely in one-dimensional helium.

Figure 10 also shows the volume excess factor β , cf. Eqs. (4.10), (4.12). Evidently the ^3He atoms do not want to be confined within the ^4He system. In order to further illustrate this, we show in Fig. 11 the $g^{34}(z)$ as a function of ρ_4 . Clearly, the correlation hole at low densities is enormous, it reaches out to beyond 100 \AA at $\rho_4=0.05 \text{ \AA}^{-1}$. A reliable

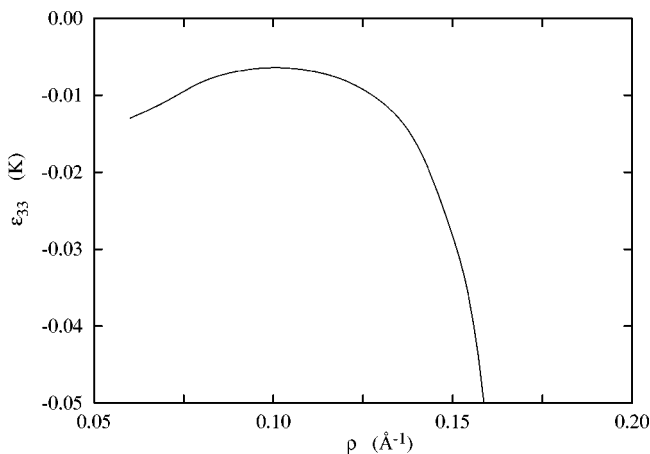


FIG. 12. The figure shows the binding energy of the ^3He - ^3He dimer as a function of density.

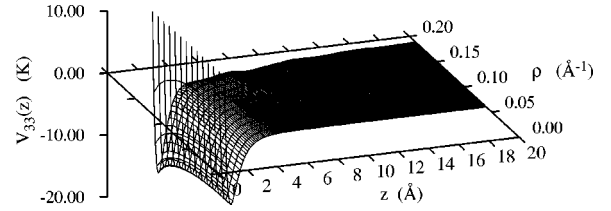


FIG. 13. The figure shows the effective interaction $V_{33}(z)$ between two ^3He impurities as a function of distance z and density.

calculation in this low-density regime requires very large sizes of the discretization volume. We have carried out our calculations in a box of length 400 \AA . We feel that, even if a numerical calculation at such box sizes is feasible, the *physical* predictions based on such a model are questionable because there is certainly no reason that the aforementioned narrow channels can be faithfully approximated by perfectly smooth tubes. Hence we have restricted ourselves to giving results for $\rho_4 > 0.05 \text{ \AA}^{-1}$ only.

Basically the same statement applies to the binding energy of two ^3He impurities. For all densities where we believe that our numerical calculation is reliable, we find, consistent with the predictions of Bashkin and collaborators,^{38,39} that there is indeed a weakly bound state of two ^3He impurities within the liquid. Since a single ^3He atom would be expelled from the system, such a scenario can be reached only if the ^4He has no free surfaces at the end of the channel. The binding energy increases rapidly with the density of the ^4He liquid, cf. Fig 12 displays the dimer binding energy as a function of density. For most of the accessible density regime, the binding energy is of the order of a few hundredths K, in other words about an order of magnitude more than the energy per particle of the ^4He background component. Figures 13 and 14 show the effective interaction $V_{33}(z)$ used in the Schrödinger equation (4.14) and the square of the ground state wavefunction, as a function of interparticle distance and density. It is evident that the effective interaction becomes more attractive with increasing density; it becomes identical to the bare potential in the low-density limit. The ^3He - ^3He dimer wave function is very broad up to a density of 0.1 \AA^{-1} , corresponding to a mean particle distance of $10\text{--}50 \text{ \AA}$. Note that there is no bound state in the zero-density limit which cannot be reached within the mixture picture due to the spinodal instability of the host ^4He liquid. The dimer state becomes reasonably localized close to the highest den-

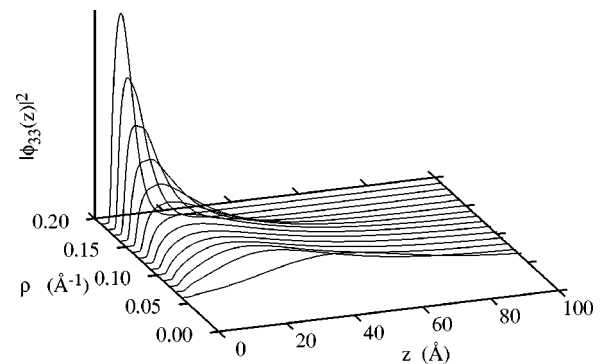


FIG. 14. Same as Fig. 13 for the square of the dimer wave function $|\phi_{33}(z)|^2$.

sity, where the binding energy increases drastically. Thus, if effects of ^3He dimerization are sought in nanotubes, experiments should be carried out at the highest possible ^4He linear densities.

V. DISCUSSION

In this paper we have reported on calculations for the properties of the ground state and low lying excitations for ^4He in one spatial dimension. We expect this to be a viable model for quasi-one-dimensional ^4He in the thin tube limit. Some evidence for this can be drawn from our calculations on quasi-two-dimensional systems, specifically adsorbed films.¹¹ In that case, the conditions under which a *quasi-two-dimensional* system such as an atomic monolayer could be treated rigorously as a two-dimensional liquid were examined. A similar comparison (i.e., a fully three-dimensional computation of ^4He in a narrow tube geometry) is today computationally feasible, however, we feel that more must be known about the particular tube wall system to warrant this effort. In this paper we assume that the walls of the tubes simply provide boundary conditions. In reality the walls will appear as an external, possibly periodic potential. We have found that at zero temperature, the ^4He will condense into a weakly bound one-dimensional liquid. The Feynman spectrum at zero-pressure is free particlelike and with increasing density smoothly develops the well-known phonon-roton shape.

In the Appendix, we sketch the derivation of the result that in one-dimension, if the low lying excitations are phonons then there is no well-defined *optimal* pair function $u_2(|z_i - z_j|)$. This in turn implies the absence of a Bose condensate.

As the density increases towards 0.19 \AA^{-1} , the inverse of the static response function shows signs of an imminent transition in the region of $k = 1.5 \text{ \AA}^{-1}$. We note that in the presence of an external periodic perturbing potential, questions of commensurate and incommensurate competing phases become an interesting possibility.

We investigated the behavior of a ^3He atom in the ^4He and showed that the minimum energy state corresponds to the single ^3He atom completely separated from the line of ^4He . In a strictly one-dimensional system of course a ^3He atom cannot move past ^4He atoms to find this minimum energy configuration. However, it is probable that these results will remain valid for the quasi-one-dimensional system where rearrangements are possible.

Finally, we showed that a pair of ^3He atoms can form a very weakly bound dimer in the presence of the one-dimensional ^4He . The dimer binding energy increases rapidly with increasing ^4He linear density and thus its presence should be most apparent at the highest attainable ^4He densities.

Note added in proof. After submission of this paper, we have learned about two diffusion Monte Carlo calculations^{44,45} that find, consistent with our predictions, long-range oscillations in the pair distribution function beyond densities of $\rho = 0.2 \text{ \AA}^{-1}$.

ACKNOWLEDGMENTS

This work was supported by the Austrian National Science Fund under Grant No. P11098-PHY. The authors would like to acknowledge many useful discussions with John Wojdylo. We also thank M. Boninsegni and M. W. Cole for discussions and communication of unpublished results.

APPENDIX DENSITY MATRIX

It is well known that the one-dimensional interacting Bose system has no Bose-Einstein condensate. Nevertheless it is useful to verify this feature for the present case; once again the importance of optimization will become apparent.

We start from the wave function (2.2) and assume, for the time being, that the two-body function $u_2(|z_i - z_j|)$ is known and is some short-ranged function in the sense that it has a Fourier transform. We then proceed to calculate the full one-body density matrix at absolute zero temperature for this wavefunction:

$$\begin{aligned} \rho_1(z, z') &= N \frac{\int dz_2 \cdots dz_N \Psi_0(z, z_2, \cdots, z_N) \Psi_0(z', z_2, \cdots, z_N)}{\int dz_1 \cdots dz_A |\Psi_0(z_1, \cdots, z_N)|^2} \end{aligned} \quad (\text{A1})$$

Working formulas for the density matrix for wave functions of the type (2.2) have been derived in several places. Following a suggestion by Feenberg, Ristig and Clark⁴⁰ performed a cumulant analysis of the density matrix (A1) and expressed $\rho_1(\mathbf{r}, \mathbf{r}')$ as a series of diagrams in terms of n -body distribution functions. Fantoni⁴¹ carried out summations of diagrams of the HNC topology. The theory was extended in Ref. 42 to inhomogeneous geometries.

Common to the earlier derivations^{40,41} was that the theory was formulated in terms of the n -body functions $u_n(\mathbf{r}_1, \dots, \mathbf{r}_n)$; but the theory can be reformulated such that it contains only physical observables. This has obvious conceptual advantages because it allows one to make direct contact to other theories such as the parquet theory of the condensate fraction which also calculate physical observables, but which are formulated without explicit reference to a wave function. It is, for the present purpose, essential because the optimal two-body function $u_2(|z_i - z_j|)$ will turn out to be an ill-defined quantity.

We do not introduce a special notation to distinguish the one-body density matrix $\rho_1(z - z')$ from its diagonal limit

$$\rho \equiv \rho_1(z, z); \quad (\text{A2})$$

the notation will be made unambiguous by explicit display of the nontrivial coordinate dependence. An especially interesting quantity is the limit of large distances $|z_1 - z_2|$,

$$\rho_1(z_1 - z_2) \rightarrow \rho n_c \text{ as } |z_1 - z_2| \rightarrow \infty. \quad (\text{A3})$$

This limit gives, in three dimensions, information about the coherent structure of the ground state.⁴³ n_c is the fraction of particles occupying the zero momentum Bose-Einstein condensate.

There is no need for the rederivation of the equations summing the diagrams contributing to the condensate fraction n_c ; they are obtained from the more general equations derived in Ref. 42 for inhomogeneous systems in the bulk limit. The final result is that

$$n_c = \exp[2D], \quad (\text{A4})$$

where the quantity D is derived by first solving the HNC equations for the momentum distribution

$$\Delta X(z) = \sqrt{g(z)} e^{\Delta N(z)} - \frac{1}{2} g(z) - \frac{1}{2} - \Delta N(z),$$

$$\Delta \tilde{N}(k) = \Delta \tilde{X}(k) [S(k) - 1], \quad (\text{A5})$$

from which one obtains

$$D = \Delta \tilde{X}(0+) - \frac{1}{2} \int \frac{dk}{2\pi\rho} \Delta \tilde{X}^2(k) S(k) [S(k) - 1]$$

$$- \frac{1}{2} \int \frac{dk}{2\pi\rho} \Delta \tilde{X}(k) [S(k) - 1]^2 + \frac{1}{8} \int \frac{dk}{2\pi\rho} \frac{[S(k) - 1]^3}{S(k)}. \quad (\text{A6})$$

The equations are valid as long as the pair distribution function has been obtained from some short-ranged $u_2(z)$. However, if the correlations are optimized, in other words if

phonons are put into the theory, then $S(k) \propto k$ as $k \rightarrow 0^+$. Then, the last term in Eq. (A6) goes to $-\infty$ and, hence $n_c = 0$ as it should be.

Finally, we return to the statement that the *optimal* two-body function $u_2(|z_i - z_j|)$ is an ill-defined quantity. In two and three dimension, an optimal $u_2(r)$ can be obtained by inverting the HNC Eq. (2.4)

$$u(r) = \ln g(r) - N(r) - E(r) \quad (\text{A7})$$

and using the optimal $g(r)$ to calculate $N(r)$ and $E(r)$. The $E(r)$ can also be calculated in 1D, however, we have

$$N(k) = \frac{[S(k) - 1]^2}{S(k)} \quad (\text{A8})$$

and, since $S(k) \propto k$ as $k \rightarrow 0^+$, the Fourier transformed $N(r)$ does not exist in one dimension. We note that, for the final formulation of the variational problem, the $N(r)$ is not necessary. But one must understand the theory in such a way that first the theory is derived for short-ranged functions $u_2(|z_i - z_j|)$, then it is reformulated in terms of quantities that are well behaved even if $S(k) \propto k$, and then one carries out the optimization. This technical subtlety occurs, of course, *only* when one insists on the Jastrow-Feenberg wave function. However, the same equations can be obtained by summing the parquet-class of Feynman diagrams where such technical difficulties do not exist.

-
- ¹E. Feenberg, *Theory of Quantum Fluids* (Academic, New York, 1969).
- ²H. Yano, S. Yoshizaki, S. Inagaki, Y. Fukushima, and N. Wada, *J. Low Temp. Phys.* **110**, 573 (1998).
- ³H. Kato, K. Ishioh, N. Wada, T. Ito, and T. Watanabe, *J. Low Temp. Phys.* **68**, 321 (1987).
- ⁴G. Stan and M. W. Cole, *Surf. Sci.* **395**, 20 (1998).
- ⁵G. Stan, V. H. Crespi, M. W. Cole, and M. Boninsegni, *J. Low Temp. Phys.* **113**, 447 (1998).
- ⁶C. E. Campbell, in *Progress in Liquid Physics*, edited by C. A. Croxton (Wiley, London, 1977), Chap. 6, pp. 213–308.
- ⁷J. W. Clark, in *Progress in Particle and Nuclear Physics*, edited by D. H. Wilkinson (Pergamon Press, Oxford, 1979), Vol. 2, pp. 89–199.
- ⁸E. Krotscheck, M. D. Miller, and J. Wojdylo, *Phys. Rev. B* **60**, 13 028 (1999).
- ⁹R. A. Aziz, V. P. S. Nain, J. C. Carley, W. J. Taylor, and G. T. McConville, *J. Chem. Phys.* **70**, 4330 (1979).
- ¹⁰E. Krotscheck, G.-X. Qian, and W. Kohn, *Phys. Rev. B* **31**, 4245 (1985).
- ¹¹B. E. Clements, J. L. Epstein, E. Krotscheck, and M. Saarela, *Phys. Rev. B* **48**, 7450 (1993).
- ¹²C. E. Campbell, *Phys. Lett. A* **44**, 471 (1973).
- ¹³C. C. Chang and C. E. Campbell, *Phys. Rev. B* **15**, 4238 (1977).
- ¹⁴E. Krotscheck, *Phys. Rev. B* **33**, 3158 (1986).
- ¹⁵E. Krotscheck and M. Saarela, *Phys. Rep.* **232**, 1 (1993).
- ¹⁶K. A. Shapiro and I. Rudnick, *Phys. Rev.* **A137**, 1383 (1965).
- ¹⁷R. A. Aziz, F. R. W. McCourt, and C. C. K. Wong, *Mol. Phys.* **61**, 1487 (1987).
- ¹⁸T. Korona, H. L. Williams, R. Bukowski, B. Jeziorski, and K. Szalewicz, *J. Chem. Phys.* **106**, 5109 (1997).
- ¹⁹C. E. Campbell, R. Folk, and E. Krotscheck, *J. Low Temp. Phys.* **105**, 13 (1996).
- ²⁰L. Castillejo, A. D. Jackson, B. K. Jennings, and R. A. Smith, *Phys. Rev. B* **20**, 3631 (1979).
- ²¹V. Apaja, J. Halinen, and M. Saarela, *J. Low Temp. Phys.* **113**, 909 (1998).
- ²²A. K. Kerman and S. E. Koonin, *Ann. Phys. (N.Y.)* **100**, 332 (1976).
- ²³P. Kramer and M. Saraceno, *Geometry of the Time-Dependent Variational Principle in Quantum Mechanics*, Lecture Notes in Physics Vol. 140 (Springer, Berlin, 1981).
- ²⁴C. C. Chang and C. E. Campbell, *Phys. Rev. B* **13**, 3779 (1976).
- ²⁵M. Saarela, *Phys. Rev. B* **33**, 4596 (1986).
- ²⁶M. Saarela and J. Suominen, in *Condensed Matter Theories*, edited by J. S. Arponen, R. F. Bishop, and M. Manninen (Plenum, New York, 1988), Vol. 3, pp. 157–165.
- ²⁷J. Suominen and M. Saarela, in *Condensed Matter Theories*, edited by J. Keller (Plenum, New York, 1989), Vol. 4, p. 377.
- ²⁸R. P. Feynman, *Phys. Rev.* **94**, 262 (1954).
- ²⁹B. E. Clements, H. Forbert, E. Krotscheck, H. J. Lauter, M. Saarela, and C. J. Tymczak, *Phys. Rev. B* **50**, 6958 (1994).
- ³⁰H. W. Jackson, *Phys. Rev. A* **4**, 2386 (1971).
- ³¹H. W. Jackson, *Phys. Rev. A* **8**, 1529 (1973).
- ³²H. W. Jackson, *Phys. Rev. A* **9**, 964 (1974).
- ³³B. E. Clements, E. Krotscheck, and C. J. Tymczak, *Phys. Rev. B* **53**, 12 253 (1996).
- ³⁴J. Bardeen, G. Baym, and D. Pines, *Phys. Rev.* **156**, 207 (1967).
- ³⁵C. Ebner and D. O. Edwards, *Phys. Rep.* **2**, 77 (1971).

- ³⁶M. Saarela and E. Krotscheck, *J. Low Temp. Phys.* **90**, 415 (1993).
- ³⁷J. C. Owen, *Phys. Rev. Lett.* **47**, 586 (1981).
- ³⁸E. P. Bashkin, *Zh. Eksp. Teor. Fiz.* **78**, 360 (1980) [*Sov. Phys. JETP* **51**, 181 (1980)].
- ³⁹E. P. Bashkin and J. Wojdylo (unpublished).
- ⁴⁰M. L. Ristig and J. W. Clark, *Phys. Rev. B* **14**, 2875 (1976).
- ⁴¹S. Fantoni, *Nuovo Cimento A* **44**, 191 (1978).
- ⁴²E. Krotscheck, *Phys. Rev. B* **32**, 5713 (1985).
- ⁴³C. N. Yang, *Rev. Mod. Phys.* **34**, 694 (1962).
- ⁴⁴M. Boninsegni and S. Moroni, *J. Low Temp. Phys.* (to be published).
- ⁴⁵M. C. Gordillo, J. Boronat, and J. Casulleras (unpublished).